Surface and nanosolid core-level shift: Impact of atomic coordination-number imperfection

Chang Q. Sun*
School of Electric and Electronic Engineering, Nanyang Technological University, Singapore 639798
(Received 25 May 2003; revised manuscript received 19 August 2003; published 12 January 2004)

Identifying the origin for core-level binding-energy shift induced by surface relaxation or nanosolid formation, and quantifying the crystal binding energy in a bulk solid has been a challenge. Here we show that a recent bond order-length-strength correlation mechanism allows us to unify the effects of surface relaxation and nanosolid formation on the core-level binding-energy shift into the atomic-coordination number imperfection. A new and simple method has been developed that enables us to elucidate the intra-atomic trapping energy (the core-level position of an isolated atom) and the crystal binding strength (core-level bulk shift) to the core electrons at the energy levels of Si and a number of metals by matching the predictions to the measurements.

DOI: 10.1103/PhysRevB.69.045105 PACS number(s): 68.35.Bs, 33.60.Fy

INTRODUCTION

Unlike the valence density of states that provides direct information about charge transportation during reaction,[1] the energy shift of a core level of an isolated atom gives profound information about the crystal binding strength that is dominated by interatomic interaction. Spontaneous processes such as alteration of the bond nature and relaxation of the bond length will affect the crystal field and hence shift the core level to a certain extent towards higher binding energy. Being able to discriminate the crystal binding (core-level shift) from the atomic trapping (core-level position of an isolated atom) of a core electron under various physical and chemical environment is a great challenge, which is beyond the scope of direct measurement using currently available probing technologies. Here we extend the recent bond-order-length-strength (BOLS) correlation mechanism,[2] to the Hamiltonian, and hence, the core-level shift of a nanosolid by including the effect of atomic coordination imperfection that induces surface relaxation and nanosolid bond contraction. Practice has led to consistent insight into the origin for the surface and nanosolid induced core-level shift and provided an effective yet simple means to determine quantitative information about the crystal binding strength and the atomic trapping energy of an isolated atom.

In addition to the well-known chemical shift caused by the core-hole screening due to charge transportation in a reaction, relaxed atomic layers at a surface can split the core level of a specimen into a few components, as illustrated in Fig. 1(a). However, the assignment for the components induced by surface relaxation is quite confusing, as summarized in Table I, due to the lack of guidelines for determining which peak arises from the surface and which one is from the bulk. With the widely used sign convention, a positive shift relates the high-energy component to the surface contribution ($S_i, i=1,2,...,B$) while the low-energy component to the bulk origin (B). The resultant peak is often located in between the components and the exact position of the resultant peak varies with experimental conditions, which is perhaps why the documented values for the core-level energy of a specimen vary from source to source. X-ray photoelectron spectroscopy (XPS) measurements[3–7] reveal that the intensity of the low-energy component often increases with the incident beam energy or with decreasing the angle between the incident beam and the surface normal in the measurement [Fig. 1(a)]. The intensity of the low-energy component also increases with decreasing the surface atomic density under the same beam condition (energy and incident angle). For example, under 390 eV beam energy, two $3d_{5/2}$ components at 334.35 and 334.92 eV have been identified from Pd(110, 100, 111) surfaces. The lower 334.35 eV peak intensity decreases with the variation of the surface geometry from (110) to (111),[8] or with the increases of atomic density ($n_{110}:n_{100}:n_{111}=1/\sqrt{2}:1:\sqrt{3}/2$). The 306.42 eV component of the Rh(111) $3d_{5/2}$-level measured under 380 eV beam energy is relatively higher than the same peak of the Rh(110) measured using 370 eV beam energy compared with the high-energy component at 307.18 eV.[8] The beam conditions and atomic density dependence of the low-energy-component intensity implies that the surface relaxation induces most likely positive shift in the XPS measurement due to the varied penetration depth of the incident beams.

Upon reacting with electronegative elements such as oxygen, the core level also splits with a production of high-energy satellite. This well-known chemical shift arises from core-hole production due to bond formation that weakens the screening of the crystal field that is acting on the specific core electrons. Chemical reaction not only alters the nature of the bond (such as from metallic to ionic) but also causes relaxation of the bond length. Interestingly, the effects of surface relaxation and chemical reaction on the core-level shift can be distinguished easily. For instance, two distinct Ru-$3d_{5/2}$ core-level components were resolved from a clean Ru(0001) surface due to the relaxation. Both components then shift up simultaneously further by up to 1.0 eV upon an addition of oxygen to the Ru(0001) surface.[19] The Rh-$3d_{5/2}$ core level of Rh(100) surface has a split of 0.65 eV relative to the main peak of the bulk, while with oxygen addition both of the components shift 0.40 eV further towards high binding energy.[23] These observations confirm that both surface relaxation and catalytic reaction could shift the core-level positively by different amount towards higher binding energy. Any spontaneously physical or chemical processes should be accompanied with binding energy enhancement

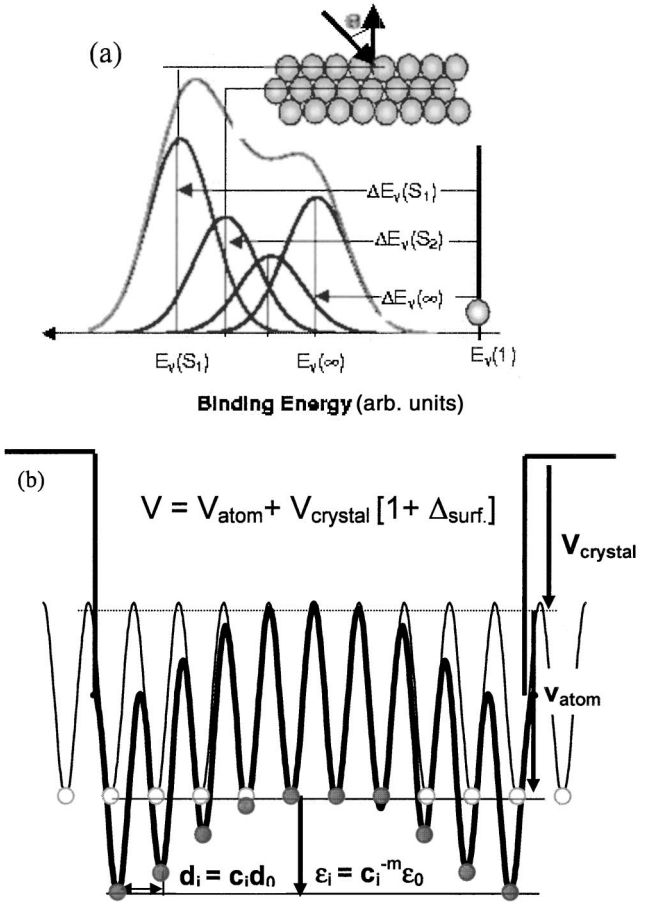

FIG. 1. (a) Illustration of the positive shift ($S_1, S_2, \ldots, B$) of the core-band components with respect to the energy level of an isolated atom, $E_\nu(1)$. $\Delta E_c(S_i) = \Delta E_c(\infty)[1+\Delta_i]$. Measurements show that the intensities of the low-energy bulk component often decreases with incident beam energy and with the increase of the angle between the incident beam and surface normal. (b) The effect of atomic CN imperfection on the bond length and intra-atomic trapping potential of the lower-coordinated atoms near the edge of a surface. The deepened intra-atomic trapping potential (v_{atom}) confines electrons to be localized in the relaxed region, which lowers the conductivity of the nanosolid. Δ_{surf} is the perturbation to the crystal potential (V_{crystal}) due to the CN-imperfection enhanced bond strength.

(or lowering of the system energy). The amount of chemical shift depends not only on the original core-level position but also on the extent of reaction.

When a solid reduces its size down to nanometer scale, the entire core-level features (both the main peak and the chemical satellites) move simultaneously towards higher binding energy and the amounts of shift depend on both the original core-level position and the particle shape and size. This has been confirmed with XPS on the size-dependence of the main core-level peaks and the oxide satellites of Cu-$2p_{3/2}$, (−932.1, −940.1 eV),[24] Sn-$3d$ (−484.4, −486.7 eV), Sn-$4d$ (−26, −31 eV), Ta-$4f_{5/2}$ (−23.4, −26.8 eV) and Ta-$4f_{7/2}$ (−31.6, −36.5 eV).[25] Compared with the monopeak of S-$2p$ and S-$2s$ core bands of a bulk solid, ZnS and CdS nanosolids exhibit three components of each the S-$2p$ and S-$2s$ core band.[26,27] These components have been ascribed as the contribution, from high to low binding energy, from the outmost capping layer (0.2–0.3 nm thick), surface layer (0.2–0.3 nm thick), and the core of the nanosolid. This specification is in accordance with the surface positive shift. The energy peak value of each component changes insignificantly with particle size but the resultant peak varies considerably with the atomic portions of the capping, the surface and the core of the nanosolid. For example, with the particle size reduction, the intensity of the core component decreases while the capping component increases, which follows the size dependence of the surface-to-volume ratio of a nanosolid. This convention has enabled an effective method of determining the particle size to be developed,[26,27] which is competent with transition electron microscopy and x-ray diffraction.

Generally, the core-level shift of a nanosolid of diameter (or thickness for a plate) D follows a scaling law: $\Delta E_C(D) = A + B/D$, where the constant A corresponds to the bulk shift, $\Delta E_C(\infty)$ with contributions from surface charging in the experiment. The slope B changes depending on surface treatment, particle dimensionality and particle–substrate interaction for supported particles.[28] The size dependent E-$2p_{3/2}$ peak shift of the Cu nanosolid deposited on HOPG (highly oriented polycrystalline graphite) and CYLC (polymer) substrates,[29] and the size dependent E-$4f$ peak shift of Au nanosolids deposited on Octanedithiol,[30] TiO_2,[31] and Pt(001)[32] substrates follow exactly the scaling law. Therefore, as physical origin (without charge transport being involved), surface relaxation and nanosolid formation play the equivalent yet unclear role in splitting and shifting the core levels of a specimen.

The underlying mechanism for the surface- and size-induced core-level shift is under debate with the following possible mechanisms:

(1) The high-energy component of the core-level shift was attributed to the surface interlayer contraction.[5,7] For Nb(001)-$3d_{3/2}$ example, the first layer spacing contracts by 12% associated with 0.50 eV core-level shift.[3] A (10 ± 3)% contraction of the first layer spacing has caused the Ta(001)-$4f_{5/2(7/2)}$ level to shift by 0.75 eV.[7] The positive core-level shift of Nb-$3d$ and Ta-$4f$ has been explained as the enhancement of the interlayer charge density and the enhancement of the resonant diffraction of the incident irradiation light due to the surface bond contraction.[3,5,7]

(2) The size-induced Cu-$2p$ core-level shift of CuO nanosolid was ascribed as the size-enhanced *ionicity* of copper and oxygen.[24] This means that an oxygen atom bonds more strongly to the Cu atoms in a nanosolid than does the oxygen atom to the Cu atoms inside the bulk.

(3) The size-enhanced Sn-$3d$, Sn-$4d$, and Ta-$4f$ core-level shift of the O–Sn and O–Ta covered metallic clusters was considered as the contribution from the *interfacial dipole* formation between the substrate and the particles.[25] The number of dipoles or the momentum of the dipole should increase with reducing particle size.

TABLE I. Specifications and the possible origins of the surface-induced core-level splitting.

Specification	Samples
($\|E_{\text{bind}}\|$:high→low)	
Positive shift $S_1, S_2, \ldots$, and B	Nb(001) (Refs. 3, 4), graphite (Ref. 5), Tb(0001) $4f$ (Ref. 6), Ta(0010) $4f$ (Ref. 7), Ta(110) (Ref. 9), Mg($10\bar{1}0$) (Ref. 10), Ga(0001) (Ref. 11)
Negative shift B, S_4, S_3, S_2, and S_1 B, S_2, S_3, S_4, and S_1	Be(000) (Ref. 12, Be($10\bar{1}0$) (Refs. 10, 13), Ru($10\bar{1}0$) (Ref. 14), Mo(110) (Ref. 15), A1(001) (Ref. 16), W(110) (Ref. 17), W(320) (Ref. 18), Pd(110, 100, 111) (Ref. 8)
Mixed shift: S_1, B, $S_{\text{dimer-up}}$, $S_{\text{dimer-down}}$ S_2, B, S_1 S_1, B, S_2	Si(111) (Ref. 19), Si(113) (Ref. 20) Ge(001) (Ref. 21) Ru(0001) (Ref. 22)

(4) The thermochemical or the initial (neutral, unionized specimen with n electrons)–final (radiation beam ionized specimen with $n-1$ electrons) states' model[4,6] defines the core-level shift as arising from the difference in cohesive energy that is needed to remove a core electron either from a surface atom or from a bulk atom. The surface atom is assumed as a $Z+1$ impurity sitting on the substrate meal of Z atomic number. The final states of atoms at a flat surface or at the curved surface of a nanosolid were expected to increase/decrease while the initial states to decreases/increase when the particle size is reduced. This model being elegantly accepted often derives the negative or mixed surface shift in theoretical calculations.

(5) Experimental investigations[33] show that the initial–final states effects cannot explain all the observations and that a metal-to-nonmetal transition mechanism was suggested to occur with a progressive decrease in cluster size.[34] The increase in the core-level binding energy in small particles was also attributed to the poor screening of the core-hole and hence a manifestation of the size-induced metal–nonmetal transition that happens at particle size in the range of 1–2 nm diameter consisting of 300 ± 100 atoms.[35]

Briefly, results show that surface relaxation and nanosolid formation share common yet unclear origin in splitting and shifting the core level to higher binding energy. However, definition of the components is quite confusing and the origin for the surface and size-induced core-level shift is highly disputed. Therefore, consistent understanding of the effect of surface relaxation and nanosolid formation on the core-level shift is therefore highly desirable. The objective of this work is to show that the recent BOLS correlation mechanism[36,37] enables us to identify the impact of atomic CN imperfection and the associated rise of binding energy density in the relaxed surface region on the electronic properties of a surface and a nanosolid.

THEORY

BOLS correlation

The significance of a flat or a curved surface is the termination of the lattice periodicity in the surface normal. Such a lattice termination not only creates a potential barrier at the surface but also reduces the CN of the surface atoms. The potential barrier confines electrons or holes moving inside the solid. The CN imperfection of an atom results in the remaining bonds of the lower-coordinated atom to contract spontaneously[38] associated with magnitude increase of the binding energy.[2] The bond strength enhancement contributes not only to the atomic cohesive energy (E_{coh}, single bond energy multiplies the atomic CN) of the specific atom but also to the energy density in the relaxed surface region. The atomic cohesive energy contributes to the Gibbs free energy that determines the thermodynamic behavior of the system such as critical temperatures for magnetic phase transition[39] and solid–liquid transition[40] of nanosolids as well as the activation energy for diffusion and chemical reaction. The binding energy density perturbs the Hamiltonian of an extended solid that determines the entire band structure such as the band gap, core-level shift and bandwidth.[37] The increased surface energy density determines the surface Young's modulus and the surface stress of the system as well.[41]

The numerical expression of the BOLS correlation is given as:[36]

$$c_i(z_i)=d_i/d_0=2/[1+\exp((12-z_i)/8z_i)],$$
$$\varepsilon_i=c_i^{-m}\varepsilon_0. \tag{1}$$

The $c_i(z_i)$ formulates perfectly the atomic-CN(or z_i)—atomic-size correlation noted by Goldschmidt, Pauling, and Feibelman.[38] d_i and d_0 is the bond length of the ith atomic layer and the bulk value, respectively. m is an adjustable parameter representing the nature of the bond. For metals, $m\sim1$,[42] for compounds and alloys, $m\sim4$.[36] ε_i and ε_0 are the binding energy per coordinate at equilibrium atomic

separation for an atom in the ith atomic layer and in the bulk, respectively. The i denotes the atomic layer that is counted up to three from the outermost atomic layer to the center of the solid. The BOLS premise involves only the m value and the atomic CN of the first three atomic layers.[43] No other assumptions or freely adjustable parameters are involved. Figure 1(b) illustrates the effect of CN imperfection on the bond length and intra-atomic trapping potential of the lower-coordinated atoms near the edge of a surface. The deepened intra-atomic trapping potential well (v_{atom}) confines electrons to be localized in the relaxed surface region, which lowers the conductivity of the nanosolid. Δ_{surf} is the perturbation to the crystal potential (V_{crystal}) due to the CN-imperfection enhanced bond strength.

There exists profound evidence for the CN-imperfection induced bond contraction and its enormous effects on various physical properties of a nanosolid (see Refs. 1, 2, 36, 37, 40, and references therein). A 4%–12% contraction of the O–Cu bond has been found to form one of the four essential stages of Cu_3O_2 bonding kinetics on the O–Cu(001) surface using very-low-energy electron diffraction.[44] A 12%–14% contraction of N–Ti/Cr bond was confirmed to be responsible for enhancing the TiCrN surface stress and Young's modulus by up to 100%.[41] A 10%–12% contraction of the Fe–Fe and Ni–Ni interlayer spacings enhances the atomic magnetic momentum by 15%–29% at the Fe and Ni surfaces.[45,46] The Al(001) surface relaxation has an effect on the total bandwidth for the relaxed monolayer, which is about 1.5 eV larger than the value for the bulk truncated monolayer. The cohesive energy is increased by about 0.3 eV per atom upon relaxation.[47] Most strikingly, without triggering electron–phonon interaction or electron–hole production, scanning tunneling spectroscopy/microscopy lately probed[48] that the band gap of Si nanorods increases from 1.1 eV to 3.5 eV with decreasing the rod diameter from 7.0 to 1.3 nm and that the surface Si–Si bond contracts by ~12% from the bulk value (0.263 nm) to ~0.23 nm. These findings concur excitingly with the BOLS anticipation. Predictions based on the BOLS premise also match well to a number of other observations on the size-and-shape dependence of nanosolids. For instance, the band-gap expansion of a nanometric semiconductor has led to the reduction of dielectric constant and hence the blueshift of the photoabsorption edges of a nanometric semiconductor.[42] The cohesive energy determines the critical temperatures for nanosolid liquidization and phase transition.[39,40] The bond-contraction enhanced surface stress influences the Gibbs free energy that determines the transition behavior of the ferroelectric[49] and pyroelectric[50] properties of nanometric PbZrTi oxides. The BOLS correlation has also enabled us to determine the dimension, strength, chemical and thermal stability of a single C–C bond in carbon nanotubes,[51] as well as the stretching limit of the Au–Au bond in the gold monatomic chain[52] based on the measurement carried out at 4 K[53] and room temperature.[54]

Hamiltonian perturbation

The BOLS correlation provides perturbation to the Hamiltonian of an extended solid, which gives rise to the electron energy potential of a surface, labeled S_i, or a nanosolid with dimension D_j,

$$V(\Delta_l) = V_{\text{atom}}(r) + V_{\text{cry}}(r)[1+\Delta_l], \tag{2}$$

where

$$\Delta_l = \begin{cases} \Delta_i(S_i) = \dfrac{\varepsilon_i - \varepsilon_0}{\varepsilon_0} = c_i^{-m} - 1 & \text{(surface)}, \\ \Delta_j(D_j) = \displaystyle\sum_{i \leqslant 3} \gamma_{ij}\Delta_i & \text{(nanosolid)}, \\ \gamma_{ij} = \dfrac{D_{\text{out},i}^{\tau} - D_{\text{in},i}^{\tau}}{D_j^{\tau}} \propto \dfrac{\tau c_i}{K_j}, \quad K_j = D_j/(2d_0). \end{cases} \tag{3}$$

In conjunction with the corresponding Block wave functions, the intra-atomic trapping potential, $V_{\text{atom}}(r)$, defines the core-level position of an isolated atom, $E_\nu(1)$, while the periodic crystal potential of an extended solid, $V_{\text{cry}}(r)$, defines not only the band gap, E_G, but also the shift of the core-level energy away from the original position, $\Delta E_\nu(\infty) = E_\nu(\infty) - E_\nu(1)$. Δ_l, being independent of the particular form of the interatomic potential, is the contribution from interlayer bond contraction (Δ_i) or the contribution from the outmost two or three atomic layers. γ_{ij} is the atomic portion of the ith atomic layer over the entire nanosolid. $D_{\text{out},i}$ and $D_{\text{in},i}$ correspond to the outer and inner diameter of the ith atomic layer of d_i thick ($d_i = D_{\text{out},i} - D_{\text{in},i}$). $\tau = 1$, 2, and 3 correspond to the dimensionality of a thin plate, a rod, and a spherical dot. The $\Sigma_{i\leqslant 3}\gamma_{ij}$ drops in a D_j^{-1} fashion from unity to infinitely small when the solid dimension grows from atomic level to macroscopic scale. At the lower end of the size limit, the perturbation to the Hamiltonian of a nanosolid relates directly to the behavior of a single bond, being the cases of a surface and a monatomic chain.

$\Delta E_\nu(\infty)$ and $E_\nu(1)$

According to the band theory and the BOLS correlation, the size dependence of both the band gap $E_G(\infty)$-expansion and core-level $E_\nu(1)$-shift follows the relations ($1 = i, j$):

$$\begin{aligned} E_G(\Delta_l) &= E_G(\infty)(1+\Delta_l), \\ E_\nu(\Delta_l) - E_\nu(1) &= [E_\nu(\infty) - E_\nu(1)](1+\Delta_l), \end{aligned} \tag{4}$$

where $E_\nu(\infty) - E_\nu(1) = \Delta E_\nu(\infty)$ is independent of crystal size, surface relaxation, or chemical reaction, thus we have the relation

$$\frac{E_\nu(\Delta_l) - E_\nu(1)}{E_\nu(\Delta_{l'}) - E_\nu(1)} = \frac{1+\Delta_l}{1+\Delta_{l'}} \quad (l' \neq l). \tag{5}$$

Given an XPS profile with clearly identified $E_\nu(\Delta_i)$ and $E_\nu(\infty)$ components of a surface ($l = i = 1,2,...$), or a set XPS data collected from a certain type of nanosolids of different sizes ($l = j = 1,2,...$), one can calculate easily the atomic $E_\nu(1)$ and the bulk $\Delta E_C(\infty)$ with the relations given by Eq. (5):

$$E_\nu(1) = \frac{(1+\Delta_{l'})E_\nu(\Delta_l) - (1+\Delta_l)E_\nu(\Delta_{l'})}{\Delta_{l'} - \Delta_l} \quad (l \neq l'), \tag{6}$$

TABLE II. Calculated atomic $E_\nu(1)$, bulk shift $\Delta E_\nu(\infty)$ and the standard deviation σ for different surfaces based on available XPS database. For elemental surface, $m=1$. $z_1=4$, $z_2=6$, and $z_3=8$ are used in calculation. Refinement of the $E_\nu(S_2)$ within XPS resolution reduces the σ to $<0.1\%$, indicating the importance of accuracy in XPS calibration.

	XPS components			Calculated			Calculated based on refined $E_\nu(S_2)$			
Surface	$E_\nu(S_1)$	$E_\nu(S_2)$	$E_\nu(\infty)$	$E_\nu(1)$	$\Delta E_\nu(\infty)$	σ	$E_\nu(S_2)$ refined	$E_\nu(1)$	$\Delta E_\nu(\infty)$	σ (%)
Poly *C 1s* (Ref. 5)	284.42		284.30	283.46	0.84					
Ru(0001) $3d_{1/2}$ (Ref. 22)	280.21	280.10	279.73	276.35	3.38	1.27 (37%)	279.955	276.344	3.3856	0.003
W(110) $4f_{7/2}$ (Ref. 17)	31.50	31.36	31.19	29.00	2.18	0.22 (10%)	31.335	29.006	2.1835	0.003
Nb(100) $3d_{5/2}$ (Ref. 3)	202.80	202.44	202.31	198.85	3.45	0.86 (25%)	202.54	198.856	3.4544	0.002
Be($10\bar{1}0$) $1s$ (Ref. 13)	111.85	111.3	111.1	105.81	5.29	1.32 (25%)	111.475	105.817	5.2835	0.002
Be(0001) $1s$ (Ref. 12)	111.9	111.35	111.1	105.46	5.64	1.08 (20%)	111.48	105.465	5.6350	0.007

$$\Delta E_\nu(\infty)=E_\nu(\infty)-E_\nu(1).$$

If $l(>2)$ components are given, the $E_\nu(1)$ and the $\Delta E_C(\infty)$ should take the mean value of the $C_l^2=l!/[(l-2)!2!]$ possible combinations with a standard error σ as both of the $E_\nu(1)$ and the $\Delta E_\nu(\infty)$ are independent of particle dimension or surface relaxation. Chemical reaction changes neither these two quantities. Accuracy of the determination is subject strictly to the XPS data calibration and the bond length that may not always follow exactly Eq. (1). Nevertheless, furnished with this approach, we would be able to elucidate the core-level positions of an isolated atom and the strength of bulk crystal binding using the conventional XPS measurement.

Combining the scaling law for any measurable quantity Q with the BLOS prediction, we have a simpler form for elucidating the $\Delta E_\nu(\infty)$,[2]

$$Q(D_j)-Q(\infty)=\begin{cases} BD_j^{-1} & \text{(measurement)},\\ Q(\infty)\times\Delta_j & \text{(theory)}\end{cases} \tag{7}$$

with slope $B\equiv Q(\infty)\times\Delta_j\times D_j\cong$ constant. The $\Delta_j\propto D_j^{-1}$ varies simply with the parameter m provided known dimensionality (τ) and size (D_j) of the solid. There are only two independent variables, m and $Q(\infty)$, in the calculations. If a certain known quantity $Q(\infty)$ for the bulk such as the melting temperature $T_m(\infty)$ or the band gap $E_G(\infty)$ and the measured size dependent $Q(D)$ of the considered system are given, the m can be readily obtained by solving Eq. (6). With the determined m, any other unknown quantities $Q(\infty)$ such as the crystal binding strength, $\Delta E_\nu(\infty)$, of the same system, and hence the energy level of an isolated atom, $E_\nu(1)$, can be determined uniquely with the above relations.

RESULTS AND DISCUSSION

Surfaces

We have calculated the $E_\nu(1)$ and $\Delta E_\nu(\infty)$ values of several surfaces based on the XPS database and Eq. (6). As listed in Table II, the small σ values evidence that the BOLS correlation describes adequately the real situations and that the parameters of m and z_i represent the true situations. Interestingly, a slight refinement of the midcomponent $E_\nu(S_2)$ within the XPS resolution reduces the σ values to less than 0.1%, indicating the criticality of XPS precision and the sensitivity and reliability of the developed method. The crystal binding strength is stronger to the electrons in the outer shells than the binding intensity to the electrons in the inner shells. For example, the binding to the C($2s^2 2p^2$)-$1s$ electrons is weaker ($\sim$0.8 eV) than the binding to the Be($2s^2$)-$1s$ ($\sim$5.6 eV) electrons due to the screening effect.

Nanosolids

The $\Delta E_\nu(\infty)$ and $E_\nu(1)$ for Cu-$2p$, Au-$4f$, and Si-$2p$ were calculated by using Eq. (6). Figures 2 and 3 compare the predicted (solid) curves with the measured size dependence of the core-level shifts of these samples (scattered data). In order to find the intercepts and slopes in the scaling law, all the experimental data were linearized with the least-root-mean-square optimization method. The intercepts provide calibration of the measurement as the intercepts may contain the effect of space charging or the system error in measurement. The slopes are the major concern in the current decoding exercises. The $E_\nu(1)$ and $\Delta E_\nu(\infty)$ of Cu-$2p$ can be obtained by calculating the Cu/HOPG system with $m=1$ using Eq. (6). The reason to take $m=1$ is that Cu atoms react hardly with the carbon surface at room temperature,[55] and that $m=1$ always hold for elemental metallic solid.[2] Decoding gives rise to the atomic trapping energy $E_{2p}(1)=-931.0$ eV for an isolated Cu atom and the bulk crystal binding energy $\Delta E_{2p}(\infty)=-1.70$ eV for an extended Cu solid. Taking the obtained $\Delta E_{2p}(\infty)$ value to the simulation iteration of the measured size dependent $E_{2p}(D)$ for Cu on CYCL gives $m=1.82$, which adds the contribution from the interfacial reaction between Cu and CYCL polymer substrate to the $m=1$. For Au nanosolid, $m=1$ has been confirmed in decoding the size dependent melting temperature of An on C and on W substrates.[40] Fitting the measured $E_{4f}(D)$ of Au on Octan with $m=1$ gives the $E_{4f}(1)=-81.50$ eV for an isolated Au atom and $\Delta E_{4f}(\infty)=-2.86$ eV for the Au bulk bonding strength. Simulations

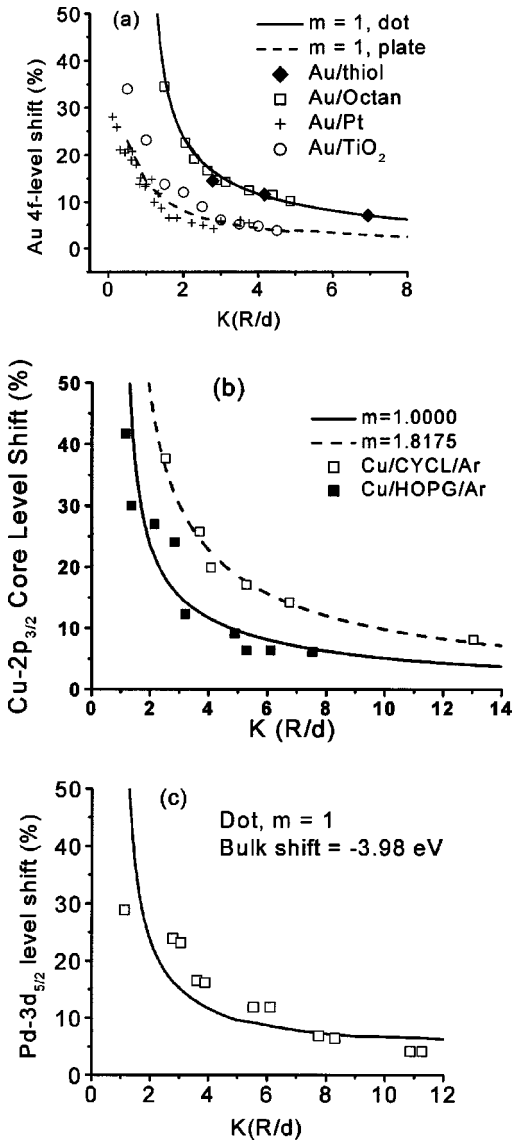

FIG. 2. Comparison of the BOLS prediction with the measured size dependence of the energy level shift. (a) Au on Octan and on Octanedithiol (Ref. 30) shows three-dimensional features while Au on TiO_2 (Ref. 31) and on Pt (Ref. 32) show more one-dimensional trend. The different m values in (b) of Cu on HOPG and CYCL (Ref. 29) indicate the contribution from the reaction between Cu nanosolid and polymer CYCL substrate. (c) Pd on HOPG substrate.

with the derived $\Delta E_{4f}(\infty) = -2.86$ eV suggested that Au growth on TiO_2 and on Pt(001) substrates proceeds more in a layer-by-layer mode, agreeing with the trend reported by the original works,[30–32] though different Au/TiO_2 growing mode has been observed.[56] However, one needs to note that the growing mode depends on the experimental conditions such as the substrate temperature and source beam energy. The deviation between prediction and measurement may be indicative of the growing mode that is in between the layer and the island growth. Simulating the XPS data of both Pd surfaces[8] and Pd nanosolids[35] led to the same value of $\Delta E_{\text{Pd-}3d}(\infty) = -4.00 \pm 0.02$ eV and $E_{\text{Pd-}3d}(1) = -330.34$ eV. For Si nanosolid, the band gap was determined first by averaging the energies of photoemission and photoabsorption to remove the electron–phonon coupling effect (or Stokes shift); simulation of the size dependent band gap expansion with the known $E_G(\infty) = 1.12$ eV gives $m = 4.88$.[57] Excitingly, the $m = 4.88$ curve for $E_G(D)$ expansion in Fig. 3(a) agrees well with the $E_G(D)$ of Si nanorods measured using STS.[48] Incorporating the derived $m = 4.88$ value into the measured size dependence of the Si-$2p$ level shift [Fig. 3(b)] gives the $E_{2p}(1) = -96.74$ eV for a Si atom and $\Delta E_{2p}(\infty) = -2.46$ eV for Si bulk binding strength. The modeling predictions agree also with the trends of core-level shift for the O–Cu, O–Sn and O–Ta, CdS, and ZnS compound nanosolids, of which both the satellites and the main peaks in the XPS profiles shift towards higher binding energy with reducing particle size. (See Table III.)

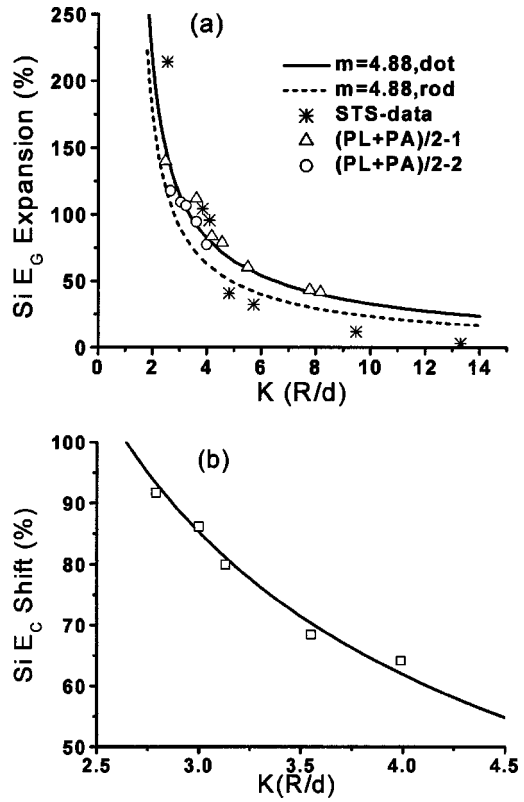

FIG. 3. Comparison of the BOLS prediction with the measured size dependence of (a) Si-E_G expansion and (b) Si-$2p$ level shift. Data 1 and data 2 were obtained using optical measurement (Ref. 57) and the STS data was obtained using STM and STS from Si nanorod (Ref. 48).

In the current modeling approach, we have found that the interfacial bond nature (character m) changes with, for instance, the Cu nanosolid-polymer substrate interfacial reaction, as shown in Fig. 2(b). For a freestanding metallic nanosolid, the metallic bond suffers from relaxation due to CN imperfection but no nature alteration if no chemical process is being involved. Metal–nonmetal transition may happen at a certain critical size, 1–2 nm. Such transition was suggested[34] to originate from the Kubo-gap (sublevel in the conduction band) expansion: $\delta = 4E_F/3N$, where E_F is the

TABLE III. The $E_\nu(1)$ of an isolated Au, Cu, and Si atom and the crystal binding energy of $\Delta E_\nu(\infty)$ obtained from decoding the $E_\nu(D_j)$ of the corresponding nanosolids.

	Au/Octan	Au/TiO_2	Au/Pt	Cu/HOPG	Cu/CYCL	Si	Pd
m		1			1.82	4.88	1
τ	3	1	1	3	3	3	3
d_0/nm		0.288		0.256		0.263	0.273
$E_\nu(\infty)$/eV		$-84.37(4f)$		$-9.32.7(2p)$		$-99.20(2p)$	$-334.35(3d)$
$E_\nu(1)$/eV	-81.504	-81.506	-81.504	-931.0		-96.74	-330.34
$\Delta E_\nu(\infty)$/eV	-2.866	-2.864	-2.866	-1.70		-2.46	-3.98

Fermi level of the bulk solid. N is the total number of atoms or conduction electrons, of the metallic nanosolid. No bond character is involved in the Kubo relation. However, from the bond relaxation perspective, the bonds near the surface region become shorter and stronger as the atomic CN and the surface curvature are reduced. The BOLS correlation [Fig. 1(b)] suggests that the effect of CN imperfection deepens the intra-atomic potential well that confines the moving electrons to be more localized, and hence, the conductivity of the metallic nanosolid becomes lower. As a complementary to the Kubo-gap expansion mechanism, the BOLS correlation may provide a scenario in real space for the conductivity reduction of a nanosolid.

CONCLUSION

The BOLS correlation premise has enabled us for the first time to unify the core-level physical shift induced by surface relaxation and nanosolid formation into the same origin of atomic CN imperfection, which should not be overlooked in dealing with the low-dimensional system. The positive shift convention assignment of the core-level components, and the specification of the capping and surface layers in CdS and ZnS nanosolid are highly favored according to the present practice. The mechanism of surface interlayer relaxation[5,7] for the surface core-level shift is also favored. The CN imperfection also enhances the iconicity of the constituents such as oxygen and metals.[24] The photovoltaic effect and the excited final states may add artifacts to the XPS spectrum that could be removed by proper calibration in measurement. The CN imperfection enhanced binding strength acts on the core electrons at the energy levels of an atom disregarding the atomic states whether it is in the neutral initial or the ionized final state. Therefore, adding the effect of CN imperfection into the initial–final states model may enhance the power of this model. Nevertheless, the developed approach has enabled us to elucidate quantitative information of the core-level position of an isolated atom and its shift due to bulk formation, which is beyond the scope of conventional approach using an XPS. Consistent understanding and the quantified information of the size dependent core-level shift of the analyzed systems gained herewith are in accordance with findings on other properties of nanosolids documented insofar by this practitioner and co-workers. Progress evidences not only the impact of atomic CN imperfection on the performance of a surface and a nanosolid but also the validity and essentiality of the BOLS correlation in describing the effect of atomic CN imperfection on the performance of a low-dimensional system.

*Email address: ecqsun@ntu.edu.sg; http://www.ntu.edu.sg/home/ecqsun/

[1] C. Q. Sun, Prog. Mater. Sci. **48**, 521 (2003).
[2] C. Q. Sun, B. K. Tay, X. T. Zeng, S. Li, T. P. Chen, J. Zhou, H. L. Bai, and E. Y. Jiang, J. Phys.: Condens. Matter **14**, 7781 (2002).
[3] B. S. Fang, W. S. Lo, T. S. Chien, T. C. Leung, C. Y. Lue, C. T. Chan, and K. M. Ho, Phys. Rev. B **50**, 11093 (1994).
[4] M. Aldén, H. L. Skriver, and B. Johansson, Phys. Rev. Lett. **71**, 2449 (1993).
[5] T. Balasubramanian, J. N. Andersen, and L. Wallden, Phys. Rev. B **64**, 205420 (2001).
[6] E. Navas, K. Starke, C. Laubschat, E. Weschke, and D. Kaindl, Phys. Rev. B **48**, 14753 (1993).
[7] R. A. Bartynski, D. Heskett, K. Garrison, G. Watson, D. M. Zehner, W. N. Mei, S. Y. Tong, and X. Pan, J. Vac. Sci. Technol. A **7**, 1931 (1989).
[8] J. N. Andersen, D. Hennig, E. Lundgren, M. Methfessel, R. Nyholm, and M. Scheffler, Phys. Rev. B **50**, 17525 (1994).
[9] D. M. Riffe and G. K. Wertheim, Phys. Rev. B **47**, 6672 (1993).
[10] J. H. Cho, K. S. Kim, S. H. Lee, M. H. Kang, and Z. Zhang, Phys. Rev. B **61**, 9975 (2000).
[11] A. V. Fedorov, E. Arenholz, K. Starke, E. Navas, L. Baumgarten, C. Laubschat, and G. Kaindl, Phys. Rev. Lett. **73**, 601 (1994).
[12] L. I. Johansson, H. I. Johansson, J. N. Andersen, E. Lundgren, and R. Nyholm, Phys. Rev. Lett. **71**, 2453 (1993).
[13] S. Lizzit, K. Pohl, A. Baraldi, G. Comelli, V. Fritzsche, E. W. Plummer, R. Stumpf, and Ph. Hofmann, Phys. Rev. Lett. **81**, 3271 (1998).
[14] A. Baraldi, S. Lizzit, G. Comelli, A. Goldoni, P. Hofmann, and G. Paolucci, Phys. Rev. B **61**, 4534 (2000).
[15] E. Lunsgren, U. Johansson, R. Nyholm, and J. N. Anderson, Phys. Rev. B **48**, 5525 (1993).
[16] R. Nyholm, J. N. Andersen, J. F. van Acker, and M. Qvarford, Phys. Rev. B **44**, 10987 (1991).
[17] D. M. Riffe, B. Kim, J. L. Erskine, and N. D. Shinn, Phys. Rev. B **50**, 14481 (1994).
[18] J. H. Cho, D. H. Oh, and L. Kleinman, Phys. Rev. B **64**, 115404 (2001).
[19] C. K. Karlsson, E. Landemark, Y. C. Chao, and R. I. G. Uhrberg, Phys. Rev. B **50**, 5767 (1994).

[20] S. M. Scholz and K. Jacobi, Phys. Rev. B **52**, 5795 (1995).
[21] T. W. Pi, J. F. Wen, C. P. Ouyang, and R. T. Wu, Phys. Rev. B **63**, 153310 (2001).
[22] S. Lizzit, A. Baraldi, A. Groso, K. Reuter, M. V. Ganduglia-Pirovano, C. Stampfl, M. Scheffler, M. Stichler, C. Keller, W. Wurth, and D. Menzel, Phys. Rev. B **63**, 205419 (2001).
[23] M. Zacchigna, C. Astaldi, K. C. Prince, M. Sastry, C. Comicioli, R. Rosei, C. Quaresima, C. Ottaviani, C. Crotti, A. Antonini, M. Matteucci, and P. Perfetti, Surf. Sci. **347**, 53 (1996).
[24] K. Borgohain, J. B. Singh, M. V. R. Rao, T. Shripathi, and S. Mahamuni, Phys. Rev. B **61**, 11093 (2000).
[25] D. Schmeißer, O. Böhme, A. Yfantis, T. Heller, D. R. Batchelor, I. Lundstrom, and A. L. Spetz, Phys. Rev. Lett. **83**, 380 (1999).
[26] J. Nanda, A. Kuruvilla, and D. D. Sarma, Phys. Rev. B **59**, 7473 (1999).
[27] J. Nanda and D. D. Sarma, J. Appl. Phys. **90**, 2504 (2001).
[28] C. Q. Sun, L. K. Pan, H. L. Bai, Z. Q. Li, P. Wu, and E. Y. Jiang, Acta Mater. **51**, 4631 (2003).
[29] D. Q. Yang and E. Sacher, Appl. Surf. Sci. **195**, 187 (2002).
[30] T. Ohgi and D. Fujita, Phys. Rev. B **66**, 115410 (2002).
[31] A. Howard, D. N. S. Clark, C. E. J. Mitchell, R. G. Egdell, and V. R. Dhanak, Surf. Sci. **518**, 210 (2002).
[32] M. Salmon, S. Ferrer, M. Jazzar, and G. A. Somojai, Phys. Rev. B **28**, 1158 (1983).
[33] V. A. Vijayakrishnan, A. Chainani, D. D. Sarma, and C. N. R. Rao, J. Phys. Chem. **96**, 8679 (1992); M. G. Mason, in *Cluster Models for Surface and Bulk Phenomena*, edited by G. Pacchioni (Plenum, New York, 1992).
[34] C. N. R. Rao, G. U. Kulkarni, P. J. Thomas, and P. P. Edwards, Chem.-Eur. J. **8**, 29 (2002).
[35] H. N. Aiyer, V. Vijayakrishnan, G. N. Subbanna, and C. N. R. Rao, Surf. Sci. **313**, 392 (1994).
[36] C. Q. Sun, S. Li, and B. K. Tay, Appl. Phys. Lett. **82**, 3568 (2003).
[37] C. Q. Sun, T. P. Chen, B. K. Tay, S. Li, H. Huang, Y. B. Zhang, L. K. Pan, S. P. Lau, and X. W. Sun, J. Phys. D **34**, 3470 (2001).
[38] V. M. Goldschmidt, Ber. Deut. Chem. Ges. **60**, 1270 (1927); L. Pauling, J. Am. Chem. Soc. **69**, 542 (1947); P. J. Feibelman, Phys. Rev. B **53**, 13740 (1996).
[39] W. H. Zhong, C. Q. Sun, B. K. Tay, S. Li, H. L. Bai, and E. Y. Jiang, J. Phys.: Condens. Matter **14**, L399 (2002).
[40] C. Q. Sun, Y. Wang, B. K. Tay, S. Li, H. Huang, and Y. Zhang, J. Phys. Chem. B **106**, 10701 (2002).
[41] C. Q. Sun, B. K. Tay, S. P. Lau, X. W. Sun, X. T. Zeng, H. Bai, H. Liu, Z. H. Liu, and E. Y. Jiang, J. Appl. Phys. **90**, 2615 (2001).
[42] C. Q. Sun, X. W. Sun, B. K. Tay, S. P. Lau, H. Huang, and S. Li, J. Phys. D **34**, 2359 (2001).
[43] For a flat or slightly curved surface, $z_1=4$, $z_2=6$, and $z_3=8$; for a spherical nanosolid, $z_1=4(1-0.75/K)$ with $K=D/2d$, being the number of atoms lined along the radius of a spherical dot or the thickness of a plate.
[44] C. Q. Sun, Surf. Rev. Lett. **8**, 367 (2001); **8**, 703 (2001).
[45] X. Qian and W. Hübner, Phys. Rev. B **60**, 16192 (1999).
[46] W. T. Geng, A. J. Freeman, and R. Q. Wu, Phys. Rev. B **63**, 064427 (2001).
[47] I. P. Batra, J. Vac. Sci. Technol. A **33**, 1603 (1985).
[48] D. D. D. Ma, C. S. Lee, F. C. K. Au, S. Y. Tong, and S. T. Lee, Science **299**, 1874 (2003).
[49] H. Huang, C. Q. Sun, T. S. Zhang, and P. Hing, Phys. Rev. B **63**, 184112 (2001).
[50] H. Huang, C. Q. Sun, and P. Hing, J. Phys.: Condens. Matter **12**, L127 (2000).
[51] C. Q. Sun, H. L. Bai, B. K. Tay, S. Li, and E. Y. Jiang, J. Phys. Chem. B **107**, 7544 (2003).
[52] C. Q. Sun, H. L. Bai, S. Li, B. K. Tay, C. Li, T. P. Chen, and E. Y. Jiang, J. Phys. Chem. B (in press).
[53] C. Untiedt, A. I. Yanson, R. Grande, G. Rubio-Bollinger, N. Agraït, S. Vieira, and J. M. van Ruitenbeek, Phys. Rev. B **66**, 085418 (2002).
[54] A. I. Yanson, G. Rubio-Bollinger, H. E. van den Brom, N. Agraït, and J. M. van Ruitenbeek, Nature (London) **395**, 783 (1998).
[55] W. F. Egelhoff, Jr., and G. G. Tibbetts, Phys. Rev. B **19**, 5028 (1979).
[56] M. Valden, X. Lai, and D. W. Goodman, Science **281**, 1674 (1998).
[57] C. Q. Sun, L. K. Pan, Y. Q. Fu, B. K. Tay, and S. Li, J. Phys. Chem. B **107**, 5113 (2003).